Supporting Information

Fabrication of coal-based oxygen-rich porous carbon nano-sheets for use in high-performance supercapacitors

Xiao-gang CHE[1], Jiao JIN[2], Yi-xiao Zhang[1], Si-yu LIU[1], Man WANG[1], Juan YANG[1,*]

（[1]*School of Chemical Engineering and Technology*, *Xi'an Jiaotong University*, *Xi'an* 710049, *China;*

[2]*Hydrocarbon High-efficiency Utilization Technology Research Center, Shaanxi Yanchang Petroleum (Group) Co., Ltd, Xi'an* 710075, *China*)

Corresponding author： YANG Juan, Ph.D, Associate Professor. E-mail: juanyang@xjtu.edu.cn

Author introduction： CHE Xiao-gang, Master student. E-mail: 13115063021@163.com

Electrochemical measurement details

The symmetrical supercapacitors were assembled in 6 M KOH aqueous electrolyte with two identical working electrodes and cellulose separator. The specific capacitance of the electrode materials in the two-electrode system was calculated by the following formula:

$$Cs = \frac{4I\Delta t}{m\Delta V} \quad (1)$$

where C_s (F g^{-1}) is the specific capacitance of electrodes in two-electrode system, I (A) is the discharge current, Δt (s) is discharge time, m (g) is the total mass of the two electrodes, and ΔV (V) is the voltage window.

The energy density E (Wh kg^{-1}) and power density P (W kg^{-1}) based on the total mass of the two electrodes were calculated according to the following equations:

$$E = \frac{Cs}{2\times 4\times 3.6}V^2 \quad (2)$$

$$P = \frac{3600E}{t} \quad (3)$$

where C_s (F g^{-1}) is the specific capacitance of electrodes in two-electrode system, V is the cell voltage and t (s) is discharge time.

Table S1 Industrial analysis and Elemental analysis of coal residual (CR)

Industrial analysis (wt%, ad[a])				Elemental analysis (wt%, ad[a])				
Mad	Aad	Vad	FCad	C(%)	O (%)	N (%)	H(%)	S(%)
0.24	18.56	45.02	36.18	74.18	18.556	2.03	3.74	1.494

[a]Air dried base

The Industrial analysis and Elemental analysis of CR were performed according to GB/T 212-2008 and GB/T 476-2008, where the determination of oxygen elements was obtained by differential subtraction.

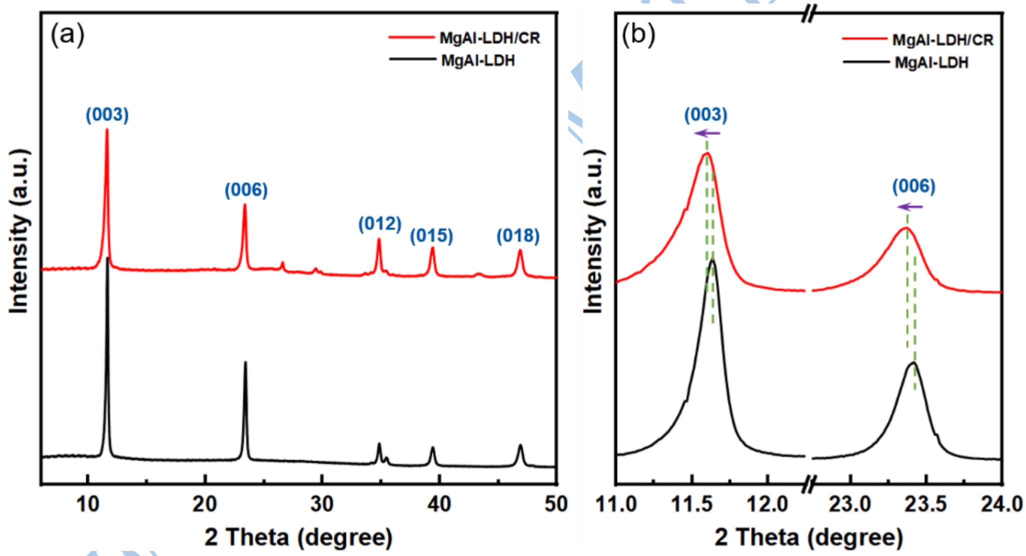

Fig. S1 (a-b) XRD patterns of MgAl-LDH/CR precursors. Two characteristic peaks at 2θ of 11.63° and 23.42° can be corresponded to the (003) and (006) crystal planes of MgAl-LDH (PDF No.89-0460), respectively. It can be found that the two characteristic peaks of the MgAl-LDH/CR precursor have a left shift in comparison to MgAl-LDH, indicating the expansion of its layer spacing and the intercalation of CR species.

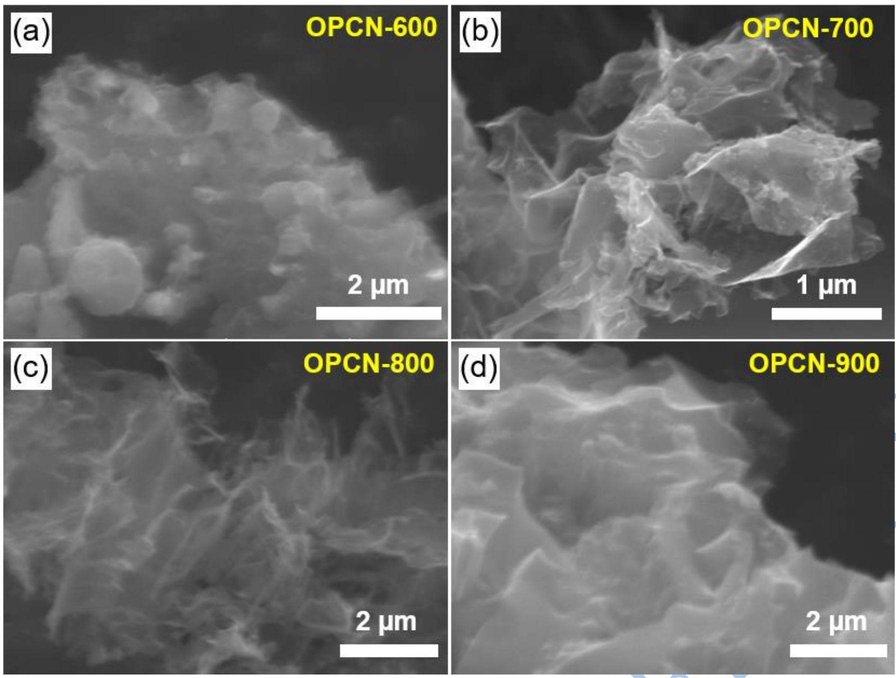

Fig. S2 SEM images of (a) OPCN-600, (b) OPCN-700, (c) OPCN-800 and (d) OPCN-900.

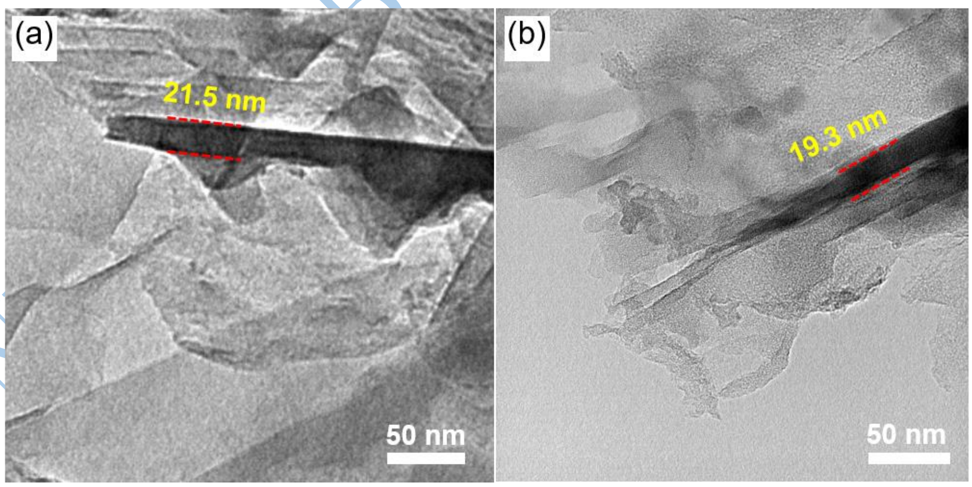

Fig. S3 (a, b) TEM images of OPCN-700.

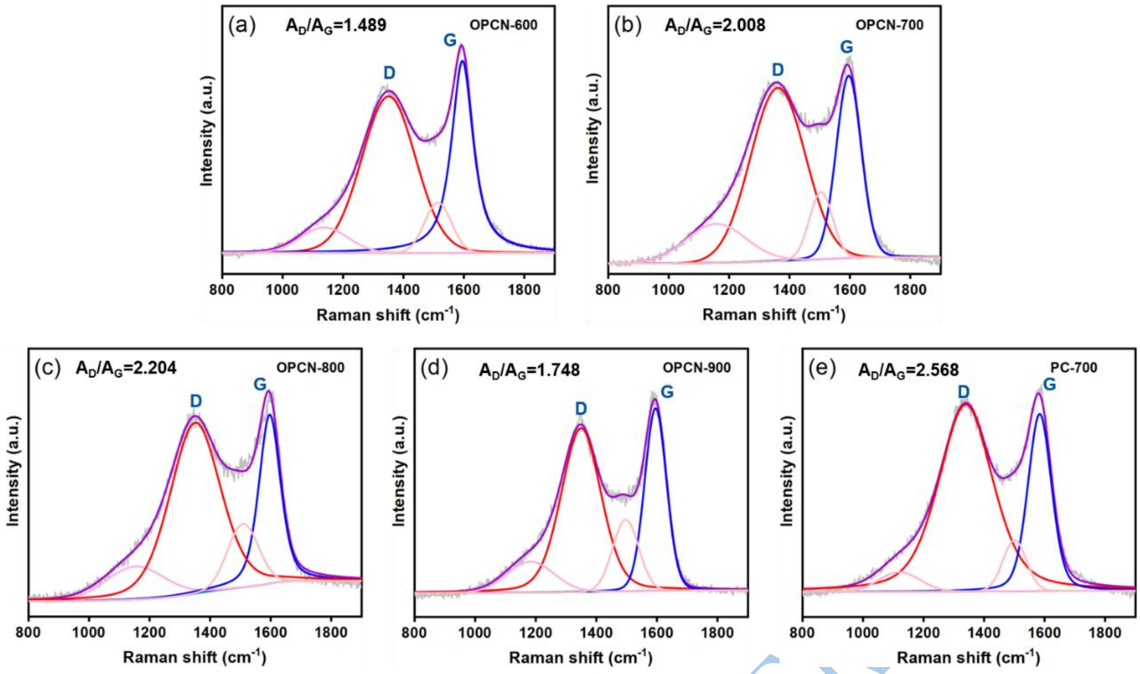

Fig. S4 (a-e) The fitted Raman spectra for OPCN-*x* and PC-700.

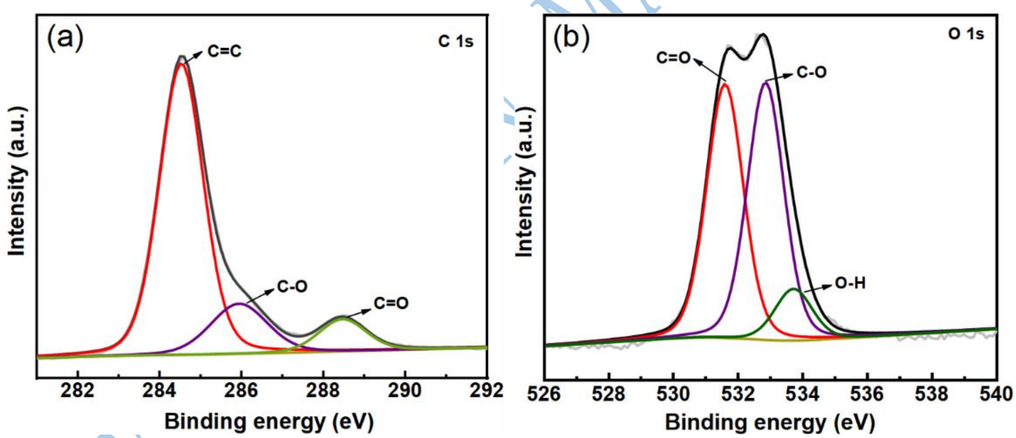

Fig. S5 (a) C 1s and (b) O 1s high-resolution spectra of PC-700 sample. The C 1s can be fitted to three characteristic peaks of C=C (284.6 eV), C-O (285.9 eV) and C=O (288.5 eV), and the fitted splitting of the O 1s spectrum yields C=O (531.6 eV), C-O (532.9 eV) and O-H (533.7 eV).

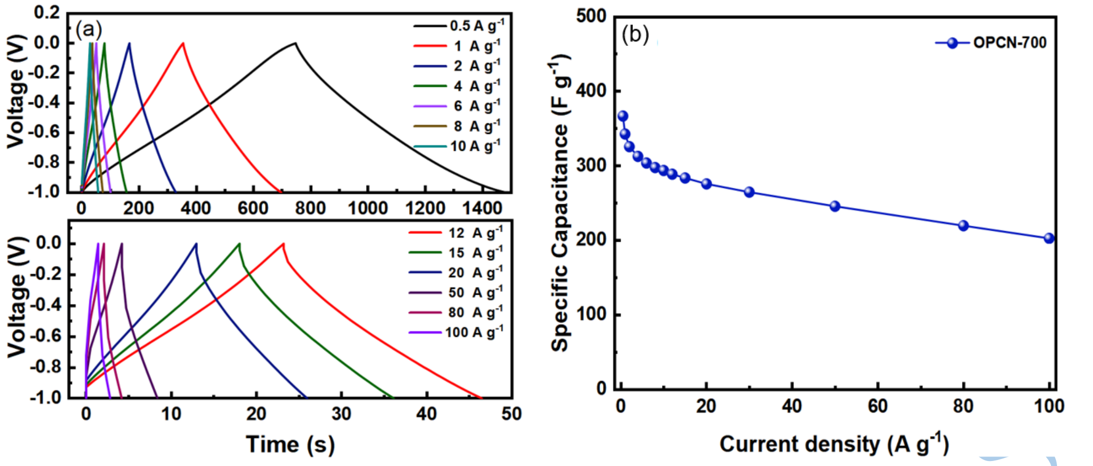

Fig. S6 (a) GCD curves and (b) the specific capacitances of the OPCN-700 at different current densities.

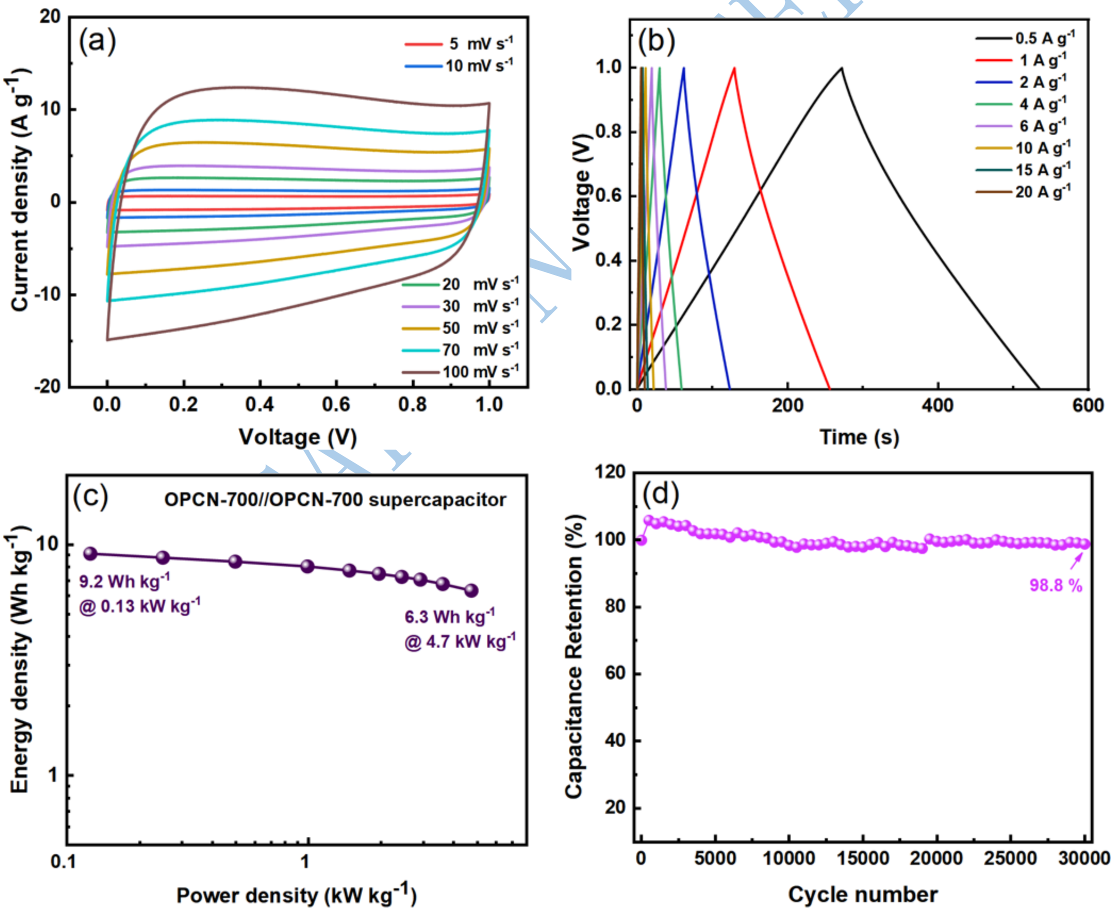

Fig. S7 (a) CV curves at different scan rates, (b) GCD profiles at various current densities, (c) Ragone plot, and (d) cycling performance of OPCN-700 based on the two-electrode cell.